

Helium Enhancement in the metal rich red giants of ω Centauri

B. P. Hema¹, Gajendra Pandey¹, R. L. Kurucz², and C. Allende Prieto³

¹ Indian Institute of Astrophysics, Koramangala II Block, Bengaluru, Karnataka,
India-560034

² Harvard-Smithsonian Center for Astrophysics, Cambridge, MA, 02138, USA

³ Instituto de Astrofísica de Canarias, 38205 La Laguna, Tenerife, Spain ; Departamento de
Astrofísica, Universidad de La Laguna, 38206 La Laguna, Tenerife, Spain

Received _____; accepted _____

ABSTRACT

The helium-enriched (He-enriched) metal-rich red giants of ω Centauri, discovered by Hema & Pandey using the low-resolution spectra from the Vainu Bappu Telescope (VBT) and confirmed by the analyses of the high-resolution spectra obtained from the HRS-South African Large Telescope (SALT) for LEID 34225 and LEID 39048, are reanalysed here to determine their degree of He-enhancement/hydrogen-deficiency (H-deficiency). The observed MgH band combined with model atmospheres with differing He/H ratios are used for the analyses. The He/H ratios of these two giants are determined by enforcing the fact that the derived Mg abundances from the Mg I lines and from the subordinate lines of the MgH band must be same for the adopted model atmosphere. The estimated He/H ratios for LEID 34225 and LEID 39048 are 0.15 ± 0.04 and 0.20 ± 0.04 , respectively, whereas the normal He/H ratio is 0.10. Following the same criteria for the analyses of the other two comparison stars (LEID 61067 and LEID 32169), a normal He/H ratio of 0.10 is obtained. The He/H ratio of 0.15-0.20 corresponds to a mass fraction of helium ($Z(\text{He})=Y$) of about 0.375-0.445. The range of helium enhancement and the derived metallicity of the program stars are in line with those determined for ω Cen's blue main-sequence stars. Hence, our study provides the missing link for the evolutionary track of the metal-rich helium-enhanced population of ω Centuari. This research work is the very first spectroscopic determination of the amount of He-enhancement in the metal-rich red giants of ω Centauri using the Mg I and MgH lines.

Subject headings: globular clusters: general — globular clusters: ω Centauri (NGC 5139), Stars: Chemically Peculiar

1. Introduction

ω Centauri, the largest and brightest milky way globular cluster is well known for hosting multiple stellar populations. The cluster’s metallicity is in the range $\sim -2.5 < [\text{Fe}/\text{H}] < \sim -0.5$ (Norris et al. 1996; Suntzeff & Kraft 1996; Lee et al. 1999; Pancino et al. 2000; Sollima et al. 2005; Johnson & Pilachowski 2010).

The survey was conducted to identify the hydrogen-deficient (H-deficient) stars in the globular cluster ω Cen (Hema & Pandey 2014) using the metal-rich ($[\text{Fe}/\text{H}] > -1$) giants of ω Cen. The low-resolution spectra for the survey were obtained from the Vainu Bappu Observatory in Kavalur, India. The analysis was based on the strengths of the (0,0) MgH band and the Mg *b* lines in the observed giant’s spectrum. The Mg abundance derived from the MgH band was found to be two times or more lower than the average Mg abundance from Mg I lines of ω Cen giants (Norris & Da Costa 1995). This discrepancy in the Mg abundance from the MgH band and that from the Mg I lines is attributed to the lower hydrogen abundance or helium enrichment, if not due to the uncertainties in the stellar parameters.

The above study was confirmed by analysing the high-resolution optical spectra of these giants obtained from the SALT observatory (Hema et al. 2018). Note that high-resolution spectra were obtained for two of the four H-deficient or He-enhanced giants discovered in our low-resolution spectroscopic survey (Hema & Pandey 2014). By deriving the Mg abundances from clean Mg I lines and from the subordinate lines of the (0,0) MgH band, Hema et al. (2018) confirm that there a discrepancy exists in the Mg abundances derived from these two indicators. This discrepancy, if not due to the uncertainties in the star’s derived effective temperature and surface gravity, is then due to the less hydrogen or more helium in the star’s atmosphere.

In this paper we present the procedure for estimating the amount of H-deficiency/He-

enhancement in a star’s atmosphere by adopting model atmospheres with normal and differing He/H ratios. The observations, the abundance analysis procedure, and the adopted model atmospheres are described in the following sections. The results are discussed in the light of He-enrichment in ω Cen.

2. Observations

The high-resolution optical spectra were obtained using Southern African Large Telescope (SALT) – high resolution spectrograph (HRS)¹. These spectra obtained with the SALT-HRS have a resolving power, $R (\lambda/\Delta\lambda)$ of 40000. The spectra were obtained with both the blue and red cameras using $2K \times 4K$ and $4K \times 4K$ CCDs, respectively, spanning a spectral range of 370–550 nm in the blue and 550–890 nm in the red.

The spectral reductions were carried out using the IRAF² (Image Reduction and Analysis Facility) software. The traditional data reduction procedure, including bias subtraction, flat-field correction, spectrum extraction, wavelength calibration, etc., was followed. The extracted and wavelength-calibrated 1D spectra were continuum normalized. The region of the spectrum with maximum flux points and free of absorption lines was considered for continuum fitting with a smooth curve passing through these points. Each of our program star was observed for about 30 minutes exposure in red and blue camera. To improve the signal-to-noise ratio, the observed spectra of the program stars were smoothed such that the strengths of the spectral lines are not altered. The signal-to-noise ratio per

¹SALT HRS is a dual beam fibre-fed, white-pupil, echelle spectrograph, employing VPH gratings as cross dispersers.

²The IRAF software is distributed by the National Optical Astronomy Observatories under contract with the National Science Foundation.

pixel, in the continuum, is 150 for the smoothed blue spectra of the program stars at about 5000Å and ~ 200 for red spectra at about 7000Å. Since there is an overlap of wavelengths, the spectrum is continuous without gaps in the blue as well as in the red spectral range. The atlas of high-resolution spectrum of Arcturus (Hinkle et al. 2000) was used as a reference for continuum fitting and also for identifying the spectral lines (Hema et al. 2018).

3. Abundance Analysis

The processed observed spectrum, as explained above, was used for conducting the abundance analysis.

The equivalent widths for several clean lines, weak and strong, were measured using the tasks in the IRAF software package. Using the measured equivalent widths, and the LTE line analysis and spectrum synthesis code MOOG (Snedden 1973) combined with model atmospheres, the stellar parameters: effective temperature, surface gravity, and microturbulence, were determined. The ATLAS9 (Kurucz 1998) plane parallel, line-blanketed LTE model atmospheres were adopted for the analysis. The derived abundances using MOOG are based on the adopted model atmosphere’s He/H ratio. The input abundances of H and He provided to MOOG, that adopts a model atmosphere computed for a normal He/H ratio of 0.1, are $\log \epsilon (\text{H})=12$ and $\log \epsilon (\text{He})=11$, respectively. Nevertheless, the input abundances of H and He provided to MOOG are $\log \epsilon (\text{H})=11.894$ and $\log \epsilon (\text{He})=11.195$, respectively, if a model atmosphere of He/H ratio 0.2 is adopted for analysis. The abundances for H and He were as usual calculated for different He/H ratios, assuming H and He as the major constituents of the stellar composition and all other elements are only in trace amounts. For example, if He/H ratio of 0.2 is adopted, then $\log \epsilon (\text{H})=11.894$ and $\log \epsilon (\text{He})=11.195$ are obtained using the standard relation: $n_{\text{H}} + 4 n_{\text{He}} = 10^{12.15}$. Similarly, for He/H ratio of 0.15, $\log \epsilon (\text{H})=11.945$ and $\log \epsilon (\text{He})=11.121$ are

obtained.

The procedure for determining the stellar parameters for the program stars is described and executed in Hema et al. (2018). The complete linelist used for the abundance analysis and the line-by-line abundances are given in TABLE 2 of Hema et al. (2018). Hema et al’s determination of stellar parameters for the analysed stars are in excellent agreement with those derived by Johnson & Pilachowski (2010). Hence, the stellar parameters for the current study have been adopted from Hema et al. (2018).

3.1. Mg abundance: MgH band and the Mg I lines

Our region of interest is the blue degraded (0,0) MgH band extending from 5330 to 4950 Å with the band head at 5211Å and the Mg *b* lines at 5167.32Å, 5172.68Å, and 5183.60Å. From Hema & Pandey (2014); Hema et al. (2018) study, based on the strengths of the MgH band and the Mg *b* lines in the observed low-resolution spectra, four stars were identified with having strong Mg *b* lines but weaker/weakest (0,0) MgH band than expected for their stellar parameters. The low-resolution spectra were obtained from the Vainu Bappu Telescope in Kavalur, India. The stars were divided into three groups based on the strengths of the Mg *b* lines and the MgH band. The first group corresponds to metal rich stars having strong Mg *b* lines and strong MgH band, the second group include metal poor stars having weak Mg *b* lines and a weak MgH band, and the third group are metal rich stars having strong Mg *b* lines with a weak MgH band, in their observed low-resolution spectra. The stellar parameters for the program stars were derived using photometric colours (Johnson and Strömgen) by Hema & Pandey (2014) which were also in good agreement with those derived spectroscopically by Johnson & Pilachowski (2010). The spectra were analysed using the spectrum synthesis code *synth* in MOOG. The analysis was carried out by comparing the Mg abundances derived from the subordinate lines of

the MgH band with that of the average Mg abundance derived for the red giants of ω Cen using Mg I lines (Norris & Da Costa 1995). The Mg abundances derived from the MgH band are expected to be same with that derived from Mg I lines. If there is a discrepancy in the derived Mg abundances, and if the difference is not due to the uncertainties in the stellar parameters, then the observed MgH band weaker than expected is attributed to the atmosphere’s lower hydrogen abundance than normal.

Two metal rich stars from the first group (LEID 39048 and LEID 60073) and two metal rich stars from the third group (LEID 34225 and LEID 35201) were identified with having stronger Mg *b* lines and weaker MgH band than expected for their effective temperatures (Hema & Pandey 2014; Hema et al. 2018). For one of the first group (LEID 34225) and one from the third group (LEID 39048), along with their comparison stars (LEID 61067 and LEID 32169), high-resolution spectra from the SALT observatory were obtained. Using the spectrum synthesis technique, described in Section 3 of Hema & Pandey (2014), the spectra were analyzed. A detailed abundance analysis has been carried out by Hema et al. (2018) for the two program stars (LEID 34225 and LEID 39048) along with their comparison stars (LEID 61067 and LEID 32169). Using the measured equivalent widths, the stellar parameters and the elemental abundances were derived. For these four stars (two program and their two comparison stars), the Mg abundance from the weaker Mg I lines were derived and contrasted with that derived from the subordinate lines of the MgH band.

The Mg abundance derived for two comparison stars, which were identified as normal Hema & Pandey (2014), have the same Mg abundance from the Mg I lines as well as from the weaker subordinate lines of the MgH band within the uncertainties. But, for the two identified H-poor stars (here program stars: LEID 34225 and LEID 39048), the difference in the Mg abundance from the Mg I and that from the MgH band is greater than 0.3 dex (see Table 6 of Hema et al. (2018)). All sources of uncertainties were explored and confirmed

that this discrepancy is not reconcilable by changing the stellar parameters within the uncertainties. Since the Mg abundance for the program stars is fixed from the weak Mg I lines, this difference cannot be attributed to the Mg abundance forming the MgH band but to the hydrogen abundance.

Hence, in this paper, model atmospheres with differing He/H ratio than normal are used to determine the degree of He-enrichment or H-deficiency in the star’s atmosphere.

3.2. Model atmospheres

The observed spectra of the program stars were reanalysed using model atmospheres with differing He/H ratios computed by one of us (RLK).

We produced one-dimensional ATLAS12 opacity-sampling model atmospheres for the range of effective temperatures and gravities, scaled-solar metal abundances, and the helium abundances appropriate for this analysis. ATLAS12 is described in Kurucz (2014). The atomic and molecular line lists were described in Kurucz (2017) and again in Kurucz (2018).

In addition to this, we wrote scripts³ that iterate and generate Kurucz LTE plane

³Model atmospheres with varying He/H ratios were computed using ATLAS9 (Kurucz (1993) and subsequent updates), in particular the version of the code set up to compile and run in gnu-linux by Sbordone (2005); Sbordone et al. (2004, 2007), (<http://atmos.obspm.fr/>). The line opacities used are those provided in the ODFs distributed with the code (tagged as NEWODF; Castelli & Kurucz (2003), and the solar reference metal mixture is that of Grevesse & Sauval (1998). For convenience the code was run using a Perl wrapper that sets up the relevant input/output files and iterates until the models converge.

parallel model atmospheres with a fine grid in He/H ratios from the above discussed coarse grid of model atmospheres.

3.3. Determination of the He/H ratio

The stellar parameters, effective temperature= T_{eff} , surface gravity= $\log g$ and microturbulence= ξ , for the program stars are from Hema et al. (2018). The adopted model atmospheres by Hema et al. (2018) for deriving stellar parameters are of normal He/H ratio 0.10. The stellar parameters were rederived using a grid of model atmospheres with He/H=0.15, 0.20, 0.25, and 0.30; the adopted metallicity of the grid is fixed based on the derived metallicity of the program star from Hema et al. (2018). The procedure adopted for determining the stellar parameters is ditto as described in Section 3 of Hema et al. (2018). The rederived stellar parameters are not sensitive and almost independent of the adopted grid's He/H ratio: 0.10, 0.15, 0.20, 0.25, and 0.30.

For the program star's derived stellar parameters, synthetic spectra in the MgH band region were computed for different He/H ratios. The Mg abundances used for the above syntheses were derived from the measured equivalent widths of the weak MgI lines for the adopted model's He/H ratio. Hence, the best fit to the MgH band in the observed spectrum determines the adopted model's He/H ratio. Finally, the elemental abundances are derived for the adopted stellar parameters: T_{eff} , $\log g$, ξ , and the He/H ratio. Note that the adopted metallicity of the model atmosphere comes from the iron abundances derived from the measured equivalent widths of the Fe lines for the star in question, and is an iterative process. The results of our analyses with adoption of α -enhanced model atmospheres having $[\text{O}/\text{Fe}]=0.5$, are in excellent agreement with that of solar scaled model atmospheres having $[\text{O}/\text{Fe}]=0$.

In the case of elemental abundances derived by adopting model atmospheres with same stellar parameters but varying He/H ratios (for example, He/H=0.20 and 0.10), the abundances from the higher He/H ratios are lower than that derived from the normal. Here, decreasing the hydrogen abundance or increasing the helium abundance i.e., increasing the He/H ratio, lowers the continuous opacity per gram (Sumangala Rao et al. 2011). Hence, for the same observed strength of the spectral line, the elemental abundance has to decrease (see Table 1). In Table 1, for the program stars, the abundances derived for the normal He/H ratio of 0.10 and also for the determined He/H ratio are given. The Mg I line at $\lambda\lambda 5711\text{\AA}$ is synthesized for the program stars LEID 34225 and LEID 39048 (see Figure 1). The determination of the Mg abundance from the Mg I lines by equivalent width analysis is in good agreement with that of the synthesis of $\lambda\lambda 5711\text{\AA}$. The decrease in abundance is proportional to the amount of H-deficiency or the He-enrichment applied in the sense of He/H ratio. However, the abundance ratios remain unchanged for most of the elements with few exceptions.

Examples of the spectrum synthesis in the MgH band region for the program stars are presented in figure 2 and 3. By adopting the respective elemental abundances derived from the adopted model computed for the pair of [Fe/H] and the He/H ratio, spectra in the MgH band region were synthesized. Figure 2, for the program star LEID 34225, clearly shows that for the Mg abundance of 6.52 ± 0.02 (from Mg I lines), the best fit to the observed MgH band (mainly the subordinate lines of MgH band at about 5175\AA) is obtained for He/H ratio of 0.15. Similarly, for LEID 39048, with the Mg I abundance of 7.25 ± 0.06 , the best fit to the observed MgH band is obtained for He/H ratio of 0.20 (see Figure 3).

The He/H ratio for the program stars is determined from the observed MgH band in their spectra. Once the stellar parameters and metallicity are determined and fixed, the MgH band strength depends mainly on the atmosphere's Mg abundance and the He/H

ratio. Then, the uncertainty on the He/H ratio is primarily due to the uncertainty on the Mg abundance. Note that, the uncertainty in the Mg abundance for the program star LEID 34225 is about 0.02 dex and that for LEID 39048 is about 0.06 dex. In general, the uncertainty on the He/H ratio is about 0.04 dex.

The corresponding mass fraction for the derived He/H ratio for the program stars: LEID 34225, $\text{He}/\text{H} = 0.15 \pm 0.04$, $Z(\text{H}) = 0.625$ and $Z(\text{He}) = Y = 0.374$; LEID 39048, $\text{He}/\text{H} = 0.20 \pm 0.04$, $Z(\text{H}) = 0.555$, $Z(\text{He}) = Y = 0.445$.

For the two normal comparison stars from our previous study Hema et al. (2018), the Mg abundance derived from the Mg I lines is same as that from the MgH band within the errors. Hence, these stars have the normal value of $\text{He}/\text{H} = 0.10$.

4. Results and Discussion

The multiple stellar populations are present in almost all the studied Galactic globular clusters (GGC) (~ 60), including ω Centauri, and also in several extragalactic globular clusters (Milone et al. 2018; Marino et al. 2012, 2009, 2011b; Yong & Grundahl 2008; Milone et al. 2020). The red giant branch (RGB) of ω Centauri show a large spread in metallicity from the mean metallicity of the cluster, $[\text{Fe}/\text{H}]$: $\sim -2.5 < [\text{Fe}/\text{H}] < \sim -0.5$ (Bedin et al. 2004; Sollima et al. 2005; Johnson & Pilachowski 2010; Simpson & Cottrell 2013). Along with the complex stellar populations in these globular clusters, they also show helium enhancement among the main-sequence stars, the red giants and also the horizontal branch (HB) stars (Milone et al. 2018). The He-enhancement in the main-sequence stars of ω Centauri have been studied by Piotto et al. (2005). Similarly, a few clusters for example, NGC 2808 (Piotto et al. 2007), NGC 6752 and NGC 6397 (Milone et al. 2010, 2012, 2013), in which the main-sequence splits due to He-enhancement have been studied.

The He-enhancement among the blue horizontal branch stars have also been studied for four of NGC 6752 and six in M4 (Villanova et al. 2009; Marino et al. 2011a).

From the studies of Piotto et al. (2005) and Milone et al. (2017), there are two main-sequence branches identified among the main sequence populations in ω Centauri. They are the *red* main-sequence (rMS) and the *blue* main-sequence (bMS). From the spectroscopic studies of rMS and bMS stars, Piotto et al. have determined that the rMS stars are more metal-poor ($[M/H]=-1.57$) than the bMS stars ($[M/H]=-1.26$). According to the canonical stellar models with canonical chemical abundances, the bMS should be more metal-poor than the rMS. To account for the fact that the bMS stars are less metal-poor, the only explanation could be the helium-enhancement in their atmospheres. For their derived metallicities, the isochrones calculated using the models with different helium abundances were compared with the observed CMD of ω Cen (see Figure 7 of Piotto et al. (2005)). The bMS can be reproduced only by assuming $Y > 0.35$, that corresponds to $He/H > 0.13$. From the near infrared transition of He I at $1.08\mu\text{m}$, the direct measure of He-abundance has been obtained by Dupree et al. (2011); Dupree & Avrett (2013) for the red giants of ω Cen. These giants are metal poor having the mean metallicity of the cluster ($[Fe/H] \sim -1.7$). This provides a clue that the clusters with multiple stellar population may also host the He-enhanced population. The helium content measured in these red giants is about $Y \leq 0.22$ for one and $Y=0.39-0.44$ for another which is similar to that measured for the main-sequence stars of ω Cen.

From our study of the metal rich red giants of ω Cen, as discussed in the Sections above, the He/H ratio is determined based on no difference in the Mg abundance derived from the Mg I lines and that from the MgH band. A proper He/H ratio stellar model is identified such that the Mg abundance from the MgH band matches with that from the Mg I lines. From the analyses of the program stars, the He/H ratio estimated are

0.15±0.04 and 0.20±0.04 for LEID 34225 and LEID 39048, respectively. These correspond to a mass fraction for LEID 34225: He/H = 0.15±0.04, Z(H)=0.625 and Z(He)=(Y)=0.374, and for LEID 39048: He/H = 0.20, Z(H)=0.555, Z(He)=(Y)=0.445. For calculating the mass fraction, only hydrogen and helium are considered, as the other elements are in trace amounts.

As discussed in our previous analysis by Hema et al. (2018), our helium rich stars are similar to the bMS stars, having similar metallicities. Out of four program stars, two were helium-rich (LEID 34225 and LEID 39048) and two were normal (comparison stars: LEID 61067 and LEID 32169). In this paper, using the models with appropriate He/H ratio, the metallicities for the two helium rich program stars are determined.

Using the appropriate He/H ratio derived by the MgH band, the derived metallicities for these He-rich program stars are, for LEID 34225, He/H=0.15 (Y=0.375), [Fe/H]=−1.2, and for LEID 39048, He/H=0.20 (Y=0.445), [Fe/H]=−0.8. Hence, the newly derived metallicities, are in excellent agreement with the metallicities of the bMS stars ([Fe/H=−1.26) within the uncertainties. And, the He content from our studies for giants of ω Cen is about Y=0.375 and 0.445. These values are same as that observed for the bMS stars. This is a strong indication that, these He-enhanced stars share the same evolutionary connections. There is a metal rich population present from the MS stars through the horizontal branch stars of ω Cen (Piotto et al. 2005; Lee et al. 1999; Pancino et al. 2000; Johnson & Pilachowski 2010; Villanova et al. 2007; Cassisi et al. 2009; D’Antona et al. 2010; Bellini et al. 2010). Among these, He-enhancement is spectroscopically confirmed in the blue-MS (Piotto et al. 2005) and the red-giants of our sample (Hema & Pandey 2014; Hema et al. 2018). Presence of the multiple branches in different evolutionary stages is a strong clue for the presence of the He-enhanced population. The direct measure of helium in the He-enhanced population are also been studied in the other globular clusters of the

Galaxy such as NGC 2808 (Marino et al. 2014).

ω Cen exhibits a unique and more complex chemical enrichment. Some of the possible scenarios that could account for this enrichment would be: multiple star-formation episodes, contribution from the massive stars which would end up as Type II SNe, the mass loss by the asymptotic giant branch stars, or may be all these scenarios have played a role in producing the observed abundance pattern of MS, subgiant branch (SGB), RGB and HB stars. The observed anomalies such as the spread in the metallicity in the MS, SGB, RGB and HB, and also the enhancement in *s*-process elements would favour the occurrence of the multiple star-formation episodes. The pattern of chemical enrichment observed in the metal poor red giants may be due to the rapid evolution of massive stars which ended up as Type II SNe. The significant contribution for the enhancement of Na, Al and *s*-process elements may come from the mass loss by the RGB and AGB stars. The multiple star-formation episodes taking place at different intervals might have formed the stars with different metallicities with different stellar composition (Johnson & Pilachowski 2010; Milone et al. 2018; Marino et al. 2012).

Our discovery of He-enhanced red giants with determination of the helium-enhancement and their metallicity, is same as that of the bMS stars. Hence, bMS stars are most probably the progenitors of the metal rich subgiants, red giants and horizontal branch stars of ω Cen. Though, there are metal-poor RGB stars that are He-enhanced, the bMS stars may be the progenitors for the metal-rich He-enhanced population indicating that, these are formed at the same epoch from the same material. Hence, this also rules out the fact that only the metal-rich giants are He-enhanced. However, more studies are required to investigate the He-enhancement in the cluster stars with different metallicities in the SGB, RGB and HB. For cool stars, the technique of contrasting the Mg abundances from the Mg I lines and from the subordinate lines of the (0,0) MgH band is very promising and a novel method

to investigate the H-deficiency/He-enhancement. Our studies (Hema & Pandey 2014; Hema et al. 2018) are the first spectroscopic studies to investigate, discover and confirm the He-enhancement in the metal-rich giants of ω Centauri, providing a crucial information and a link for understanding the evolution of metal-rich He-enhanced stars.

5. Conclusions

From the discovery of the He-rich red-giants in the Galactic globular cluster ω Centauri using the low-resolution spectra (Hema & Pandey 2014), study of these giants by obtaining the high-resolution spectra for deriving the appropriate Mg abundance from the MgI to confirm the H-deficiency/He-enrichment using the MgH bands (Hema et al. 2018), and now estimating the H-deficiency/He-enrichment using the proper model atmospheres, confirms the existence of He-enhanced metal-rich red giants same as that observed for the blue main-sequence stars of ω Centauri. Our studies bridges the evolutionary track of the metal-rich He-rich population of ω Cen.

6. Acknowledgment

We thank the anonymous referee for a constructive report.

REFERENCES

- Bedin, L. R., Piotto, G., Anderson, J., Cassisi, S., King, I. R., Momany, Y., & Carraro, G. 2004, *ApJ*, 605, L125
- Bellini, A., Bedin, L. R., Piotto, G., Milone, A. P., Marino, A. F., & Villanova, S. 2010, *AJ*, 140, 631
- Cassisi, S., Salaris, M., Anderson, J., Piotto, G., Pietrinferni, A., Milone, A., Bellini, A., & Bedin, L. R. 2009, *ApJ*, 702, 1530
- Castelli, F., & Kurucz, R. L. 2003, in *IAU Symposium*, Vol. 210, *Modelling of Stellar Atmospheres*, ed. N. Piskunov, W. W. Weiss, & D. F. Gray, A20
- D’Antona, F., Caloi, V., & Ventura, P. 2010, *MNRAS*, 405, 2295
- Dupree, A. K., & Avrett, E. H. 2013, *ApJ*, 773, L28
- Dupree, A. K., Strader, J., & Smith, G. H. 2011, *ApJ*, 728, 155
- Grevesse, N., & Sauval, A. J. 1998, *Space Sci. Rev.*, 85, 161
- Hema, B. P., & Pandey, G. 2014, *ApJ*, 792, L28
- Hema, B. P., Pandey, G., & Srianand, R. 2018, *ApJ*, 864, 121
- Johnson, C. I., & Pilachowski, C. A. 2010, *ApJ*, 722, 1373
- Kurucz, R. 1993, *ATLAS9 Stellar Atmosphere Programs and 2 km/s grid*. Kurucz CD-ROM No. 13. Cambridge, 13
- Kurucz, R. L. 1998, <http://kurucz.harvard.edu/>
- . 2014, *Model Atmosphere Codes: ATLAS12 and ATLAS9*, 39–51

- . 2017, *Canadian Journal of Physics*, 95, 825
- . 2018, *Astronomical Society of the Pacific Conference Series*, Vol. 515, *Including All the Lines: Data Releases for Spectra and Opacities through 2017*, 47
- Lee, Y.-W., Joo, J.-M., Sohn, Y.-J., Rey, S.-C., Lee, H.-C., & Walker, A. R. 1999, *Nature*, 402, 55
- Marino, A. F., Milone, A. P., Piotto, G., Villanova, S., Bedin, L. R., Bellini, A., & Renzini, A. 2009, *A&A*, 505, 1099
- Marino, A. F., Villanova, S., Milone, A. P., Piotto, G., Lind, K., Geisler, D., & Stetson, P. B. 2011a, *ApJ*, 730, L16
- Marino, A. F., et al. 2011b, *A&A*, 532, A8
- . 2012, *ApJ*, 746, 14
- . 2014, *MNRAS*, 437, 1609
- Milone, A. P., et al. 2010, *ApJ*, 709, 1183
- . 2012, *A&A*, 540, A16
- . 2013, *ApJ*, 767, 120
- . 2017, *MNRAS*, 469, 800
- . 2018, *MNRAS*, 481, 5098
- . 2020, *MNRAS*, 491, 515
- Norris, J. E., & Da Costa, G. S. 1995, *ApJ*, 447, 680
- Norris, J. E., Freeman, K. C., & Mighell, K. J. 1996, *ApJ*, 462, 241

- Pancino, E., Ferraro, F. R., Bellazzini, M., Piotto, G., & Zoccali, M. 2000, *ApJ*, 534, L83
- Piotto, G., et al. 2005, *ApJ*, 621, 777
- . 2007, *ApJ*, 661, L53
- Sbordone, L. 2005, *Memorie della Societa Astronomica Italiana Supplementi*, 8, 61
- Sbordone, L., Bonifacio, P., & Castelli, F. 2007, in *IAU Symposium*, Vol. 239, *Convection in Astrophysics*, ed. F. Kupka, I. Roxburgh, & K. L. Chan, 71–73
- Sbordone, L., Bonifacio, P., Castelli, F., & Kurucz, R. L. 2004, *Memorie della Societa Astronomica Italiana Supplementi*, 5, 93
- Simpson, J. D., & Cottrell, P. L. 2013, *MNRAS*, 433, 1892
- Snedden, C. A. 1973, PhD thesis, THE UNIVERSITY OF TEXAS AT AUSTIN.
- Sollima, A., Ferraro, F. R., Pancino, E., & Bellazzini, M. 2005, *MNRAS*, 357, 265
- Sumangala Rao, S., Pandey, G., Lambert, D. L., & Giridhar, S. 2011, *ApJ*, 737, L7
- Suntzeff, N. B., & Kraft, R. P. 1996, *AJ*, 111, 1913
- Villanova, S., Piotto, G., & Gratton, R. G. 2009, *A&A*, 499, 755
- Villanova, S., et al. 2007, *ApJ*, 663, 296
- Yong, D., & Grundahl, F. 2008, *ApJ*, 672, L29

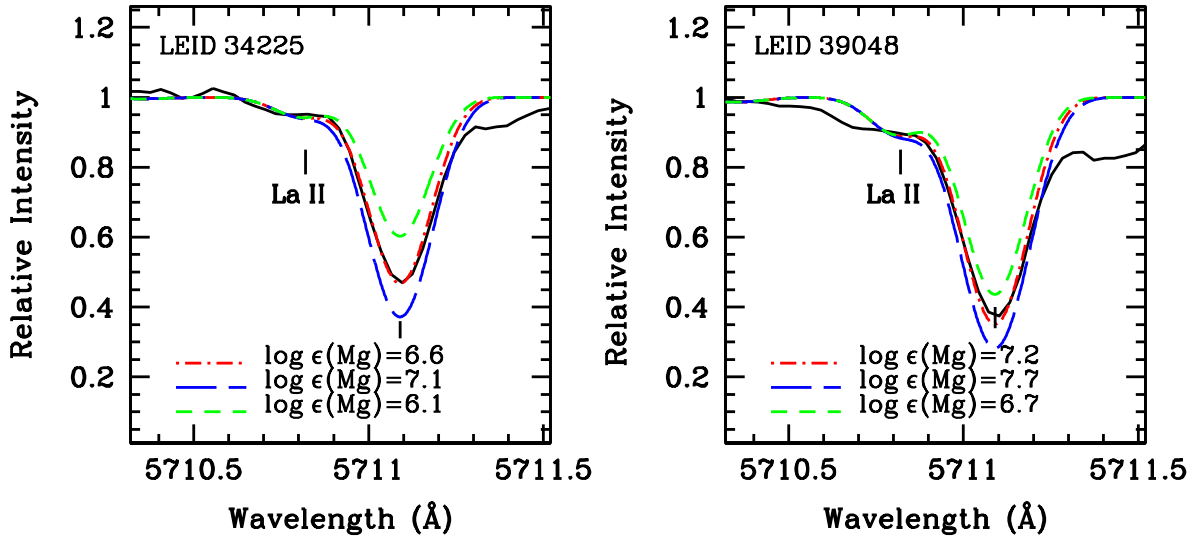


Fig. 1.— The Mg abundance derived from the $\lambda\lambda 5711\text{\AA}$ Mg I line for the program stars. The best fit synthesis is shown with the red-dash dotted line.

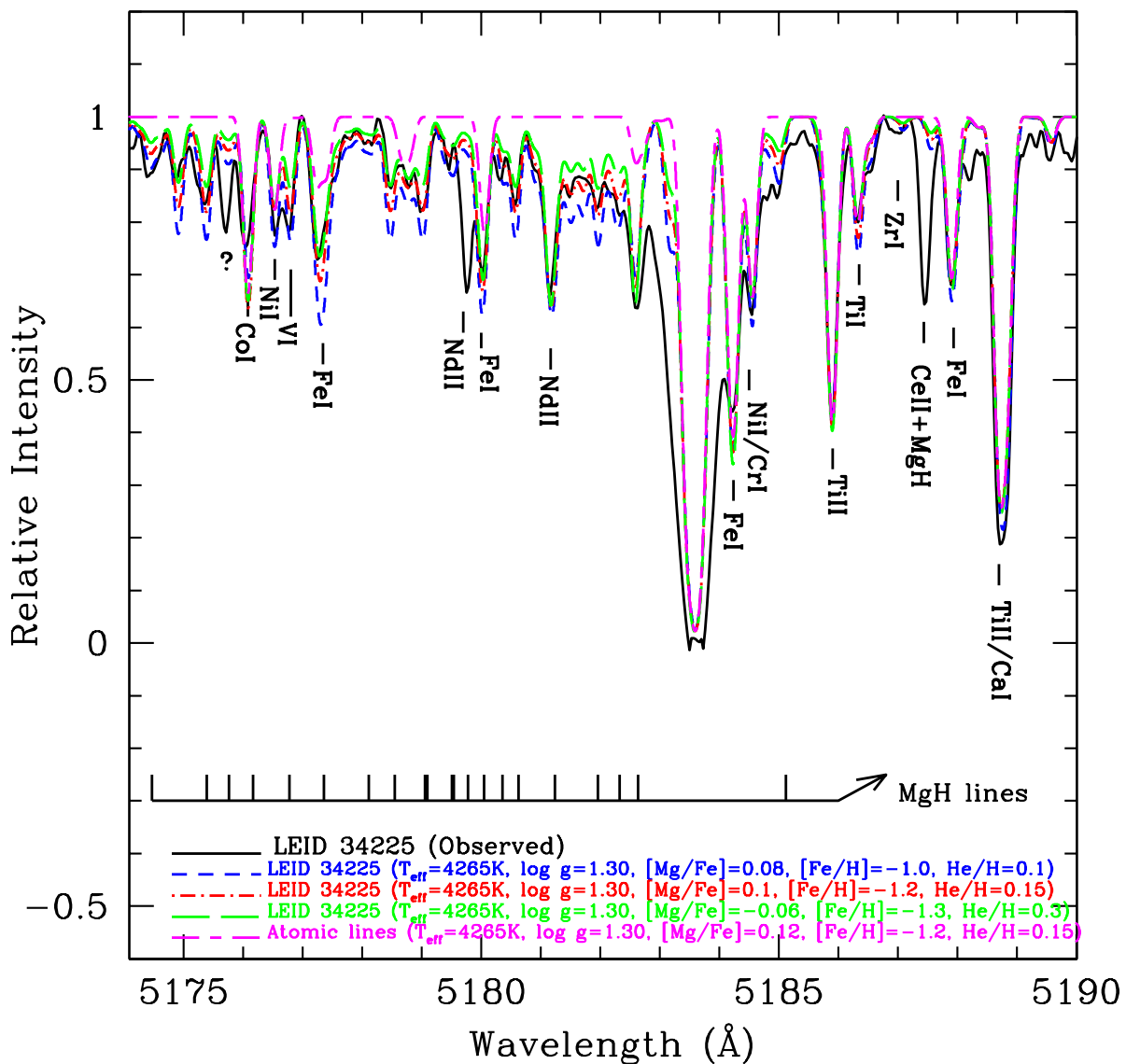


Fig. 2.— Observed and the synthesized MgH bands for LEID 34225 are shown. The spectra synthesized for the Mg abundance derived from the MgI lines and the best fit value of He/H ratio are shown in red dash-dotted line. The synthesis for the two value of the He/H are also shown.

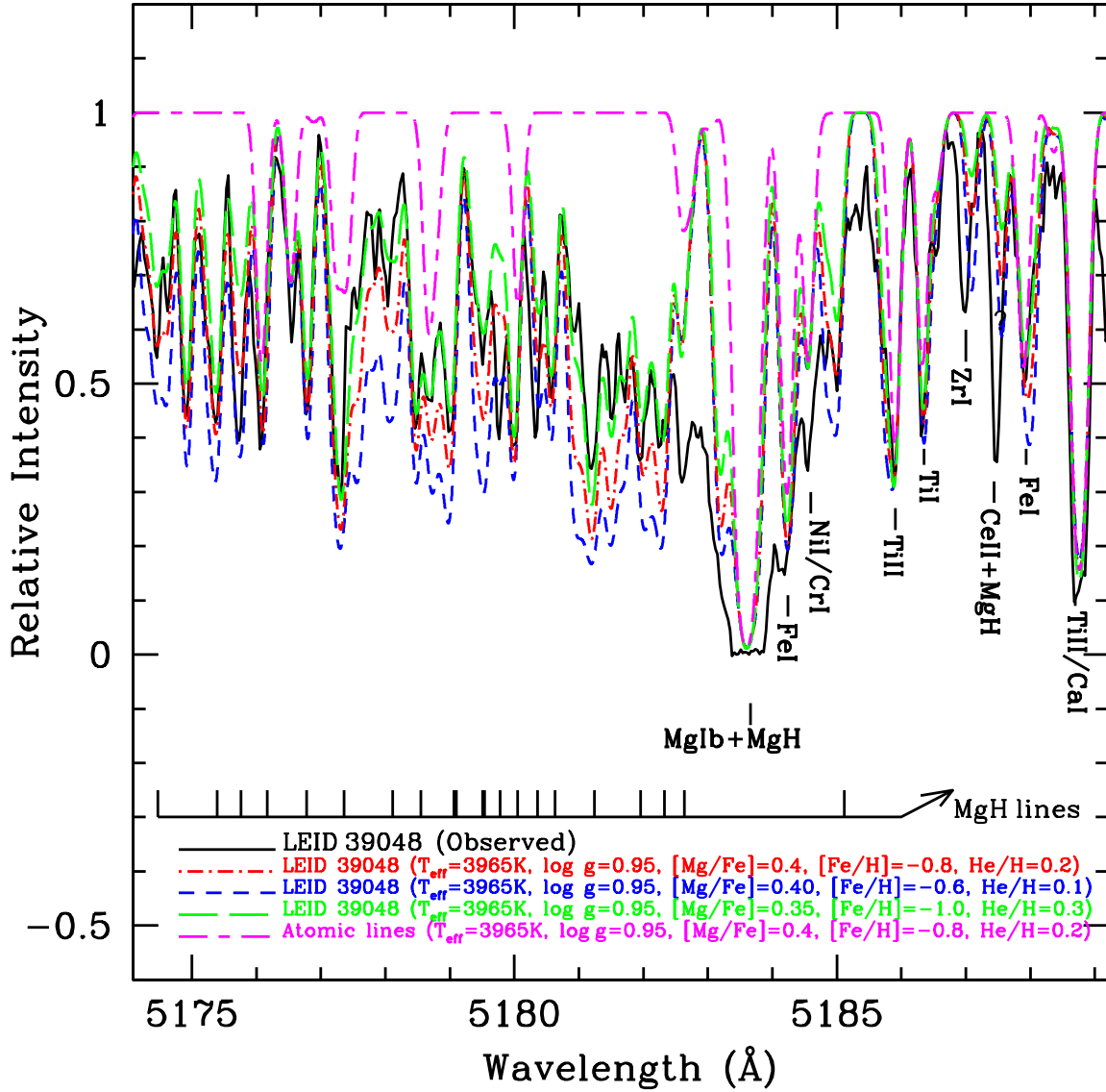


Fig. 3.— Observed and the synthesized MgH bands for LEID 39048 are shown. The spectra synthesized for the Mg abundance derived from the Mg I lines and the best fit value of He/H ratio are shown in red dash-dotted line. The synthesis for the two value of the He/H are also shown.

Table 1. Abundances for different He/H ratios

Elements	LEID 34225						LEID 39048					
	log ϵ_{\odot}	log $\epsilon(\text{He}/\text{H}=0.1)$	[X/Fe]	log $\epsilon(\text{He}/\text{H}=0.15)$	[X/Fe]	n	log $\epsilon(\text{He}/\text{H}=0.1)$	[X/Fe]	log $\epsilon(\text{He}/\text{H}=0.2)$	[X/Fe]	n	
H	12.00	12.00	...	11.945	12.00	...	11.894	
He	10.93	11.00	...	11.121	11.00	...	11.195	
O	8.69	7.4	-0.25	7.36	-0.13	1	8.1 \pm 0.06	0.03	7.99 \pm 0.07	0.10	2	
Na	6.24	5.72 \pm 0.16	0.52	5.65 \pm 0.16	0.61	4	6.50 \pm 0.04	0.88	6.38 \pm 0.04	0.94	2	
Mg (MgI)	7.60	6.65 \pm 0.05	0.09	6.52 \pm 0.02	0.12	4	7.41 \pm 0.1	0.43	7.25 \pm 0.06	0.45	5	
Mg (MgH)	...	6.26	-0.29	6.50	0.10	...	7.0	0.02	7.20	0.40	...	
Al	6.45	6.50 \pm 0.12	1.09	6.32 \pm 0.11	1.07	4	6.50 \pm 0.13	0.67	6.33 \pm 0.1	0.68	4	
Si	7.51	7.00 \pm 0.11	0.53	6.85 \pm 0.11	0.54	5	7.36 \pm 0.15	0.47	7.02 \pm 0.16	0.31	7	
Ca	6.34	5.40 \pm 0.16	0.1	5.26 \pm 0.16	0.12	9	5.9 \pm 0.08	0.18	5.82 \pm 0.08	0.28	8	
Sc I	3.15	2.24 \pm 0.16	0.13	2.20 \pm 0.14	0.25	4	
Sc II	3.15	2.25 \pm 0.09	0.14	2.13 \pm 0.09	0.18	5	2.60 \pm 0.2	0.07	2.37 \pm 0.20	0.02	5	
Ti I	4.95	4.30 \pm 0.14	0.39	4.24 \pm 0.14	0.49	7	4.80 \pm 0.17	0.47	4.80 \pm 0.17	0.67	11	
Ti II	4.95	4.29 \pm 0.11	0.38	4.14 \pm 0.11	0.39	4	
V	3.93	2.66 \pm 0.14	-0.23	2.64 \pm 0.14	-0.09	6	3.20 \pm 0.15	-0.11	3.20 \pm 0.15	0.08	8	
Cr	5.64	4.60 \pm 0.13	0.0	4.53 \pm 0.13	0.09	7	5.00 \pm 0.1	-0.02	4.92 \pm 0.11	0.08	...	
Mn	5.43	4.39 \pm 0.06	0.0	4.32 \pm 0.07	0.09	3	4.85 \pm 0.04	0.04	4.77 \pm 0.04	0.14	3	
Fe I	7.50	6.46 \pm 0.16	-1.04	6.32 \pm 0.12	-1.18	19	6.88 \pm 0.14	-0.62	6.70 \pm 0.13	-0.80	16	
Fe II	...	6.46 \pm 0.06	-1.04	6.25 \pm 0.08	-1.25	2	
Co	4.99	4.01 \pm 0.14	0.06	3.92 \pm 0.14	0.13	6	4.32 \pm 0.13	-0.05	4.14 \pm 0.11	-0.05	7	
Ni	6.22	5.13 \pm 0.09	-0.05	5.04 \pm 0.09	0.02	3	5.74 \pm 0.17	0.14	5.50 \pm 0.18	0.09	7	
La	1.10	1.10	1.04	0.95	1.05	1	1.32	0.84	1.19	0.89	1	